PERGAMON

International Journal of Multiphase Flow 28 (2002) 409–425

International Journal of Multiphase Flow

www.elsevier.com/locate/ijmulflow

Finite Reynolds number effect on the rheology of a dilute suspension of neutrally buoyant circular particles in a Newtonian fluid

Neelesh A. Patankar [a,*], Howard H. Hu [b]

[a] *Department of Mechanical Engineering, Northwestern University, 2145 Sheridan Road, Evanston, IL 60208-3111, USA*
[b] *Department of Mechanical Engineering and Applied Mechanics, University of Pennsylvania, Philadelphia, PA 19104-6315, USA*

Received 9 March 2001; received in revised form 5 August 2001

Abstract

Knowledge of suspension rheology can help in the prediction of its behavior under various flow conditions. Considerable theoretical effort has been made to model the macroscopic properties of suspensions of rigid particles in a Newtonian fluid, but for the most part it has been limited to zero particle Reynolds number. In this paper we investigate the effect of finite particle Reynolds number on the macroscopic properties of suspensions of rigid circular particles in a Newtonian fluid in the dilute limit (no interaction between particles). Two-dimensional numerical simulations are performed. Navier–Stokes equations are solved for the fluid without neglecting any terms. It is seen that the viscosity of the suspension shear thickens. The first normal stress difference is negative and increases in magnitude as the Reynolds number is increased.

Keywords: Rheology; Suspensions; Finite Reynolds number; Newtonian fluids; Particulate flows

1. Introduction

Constitutive equations represent the macroscopic behavior of a fluid. The rheology of a suspension depends on factors such as the microstructural mechanics, which includes various forces acting on the particles as well as their spatial and temporal distributions. Couette flow is an appropriate flow for such investigations.

* Corresponding author. Tel.: +1-847-491-3021; fax: +1-847-491-3915.
E-mail address: n-patankar@northwestern.edu (N.A. Patankar).

0301-9322/02/$ - see front matter
PII: S0301-9322(01)00053-2

Considerable theoretical effort has been made to model the macroscopic properties of suspensions in Newtonian fluids in terms of their microstructural mechanics. For the most part it has been limited to low concentrations at zero particle Reynolds number. This approach originated from the work of Einstein (1906) on the effective viscosity of a dilute suspension of rigid spheres. Details of this approach can be found in the review articles in this area (Batchelor, 1974, 1976; Brenner, 1974; Jeffrey and Acrivos, 1976; Russel, 1980; Davis and Acrivos, 1985; Brady and Bossis, 1988). Kang et al. (1997) studied the rheology of dense bubble suspensions. Ryskin and Rallison (1980) studied the extensional viscosity of a dilute suspension of spherical particles at intermediate microscale Reynolds numbers. Rheology of rigid particulate suspensions, in the zero Reynolds number limit at high concentrations, has been investigated using numerical simulations (see Foss and Brady, 2000 and references therein). Sangani et al. (1996) studied the effect of finite Stokes number on suspensions. Lin et al. (1970)) studied the effect of inertia on the rheology of suspensions of rigid spheres in Newtonian fluids, but their results are valid for low particle Reynolds numbers (<1) and in the dilute limit. For higher particle Reynolds numbers (>1), no results are available.

In this paper we investigate the effect of inertia on the macroscopic properties of suspensions in the dilute limit. Only the hydrodynamic force acts on the particles. We do not consider the Brownian or interparticle colloidal forces. The investigation has become possible because of our capability to simulate two-dimensional motions of small and large numbers of particles in Newtonian fluids at finite Reynolds numbers (Hu, 1996; Hu et al., 2001). We solve the full Navier–Stokes equations for the fluid and the Newton equations of motion for the particles. Details of the numerical scheme and convergence results are presented by Hu (1996).

In the literature, the flow problem is often simplified by ignoring the viscous effects completely (inviscid potential flow) or by ignoring the fluid and particle inertia completely (Stokes flow). Potential flow simulations (Sangani and Prosperetti, 1993) do resolve some mechanisms but the wake effect and the other non-linear mechanisms are absent. Brady and co-workers (Brady and Bossis, 1988; Brady, 1993) have developed a numerical technique for simulating the motion of large numbers of particles in Stokes flow. They call these the Stokesian Dynamics simulations. These simulations are appropriate for suspensions with very small particle Reynolds numbers (so that the fluid inertia may be neglected) and small Stokes numbers (so that the particle inertia may be neglected). They appear to successfully capture the hydrodynamic interaction between the particles. Researchers have investigated the case of zero Reynolds number and finite Stokes number (e.g. Koch, 1990). Marchioro et al. (2000) and Marchioro et al. (2001) have described, for the first time, a method based on numerical simulations to characterize the ensemble-average behavior of spatially non-uniform suspensions of spheres at small Reynolds numbers.

Direct numerical simulations, using the full Navier–Stokes equations coupled with Newton's equations of motion for the particles, do not neglect inertia. Inertia can become important in flows in various applications such as sedimentation columns, fluidized beds and lubricated transport of particulate mixtures through pipes, to name a few. An understanding of the effective properties of particulate mixtures in such applications can be obtained from the direct numerical simulation of solid–liquid flows.

In this paper we will first present the problem statement and then discuss expressions to calculate the bulk properties of suspensions. Results on the bulk properties of suspensions in the dilute limit will then be presented.

2. Problem statement

Consider an incompressible Newtonian fluid of density ρ and viscosity η. A rigid circular particle of radius a and density ρ is placed at the center of a unit cell with a periodic boundary condition in the axial direction. The fluid and particle densities are identical. The channel or the cell width is D and the periodic length is L (Fig. 1). Shearing motion is caused by the relative velocity between the channel walls.

The governing equations in a non-dimensional form are given by

$$\begin{aligned}
&\nabla \cdot \mathbf{u} = 0,\\
&\mathrm{Re}\left(\frac{\partial \mathbf{u}}{\partial t} + (\mathbf{u}\cdot\nabla)\mathbf{u}\right) = -\nabla p + \nabla^2 \mathbf{u},\\
&\pi Re \frac{\mathrm{d}\mathbf{U}}{\mathrm{d}t} = \oint [-p\mathbf{1} + (\nabla\mathbf{u} + (\nabla\mathbf{u})^{\mathrm{T}})]\cdot \mathbf{n}\,\mathrm{d}\Gamma,\\
&\frac{\pi}{2} Re \frac{\mathrm{d}\Omega}{\mathrm{d}t} = \oint (\mathbf{x}-\mathbf{X}) \times ([-p\mathbf{1} + (\nabla\mathbf{u} + (\nabla\mathbf{u})^{\mathrm{T}})]\cdot \mathbf{n})\,\mathrm{d}\Gamma,
\end{aligned} \tag{1}$$

where $\mathbf{u}$ is the velocity vector, p is the dynamic pressure, $\mathbf{U}$ is the translational velocity of the particle, Ω is the angular velocity, $\mathbf{1}$ is an identity tensor, $\mathbf{n}$ is the unit outward normal on the surface of the particle, $\mathbf{X}$ is the coordinate of the center of mass of the particle and $\mathbf{x}$ is the coordinate of a point on the surface of the particle. The integral terms represent the momentum exchange between the fluid and the particle. Appropriate expressions for the mass and the moment of inertia of the particle in terms of its density and radius have been substituted. No-slip boundary condition is applied on the particle surface.

In Eq. (1) we non-dimensionalize length by the radius a of the particles, velocities by Va/D, where V is the relative velocity between the two channel walls, time by D/V, angular velocity by V/D and pressure by $\eta V/D$. We use the effective shear-rate, V/D, as the reference scale.

The parameters governing the problem are

$$Re = \frac{\rho V a^2}{D\eta} \quad \text{(Reynolds number)},$$

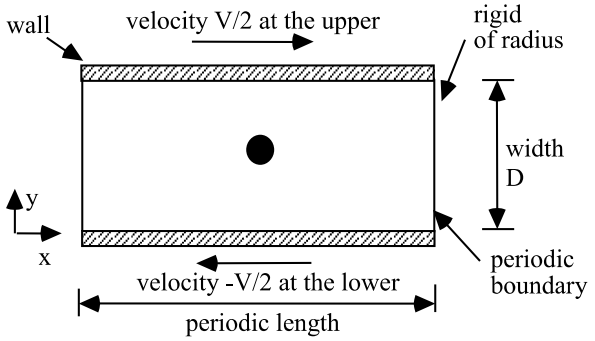

Fig. 1. Periodic unit cell for two-dimensional simulations.

$\phi = N\pi a^2/LD$ (solid area fraction).

Only the dynamic pressure is considered in Eq. (1) because the hydrostatic pressure balances the body force on the fluid as well as the neutrally buoyant particles. In order to ensure that the simulation converges to the right solution, we need to apply a boundary condition such that there is no overall gradient of the dynamic pressure along the axial direction of the periodic channel. This condition is automatically imposed by the periodic boundary condition.

3. Bulk properties of suspensions

Consider a general two-dimensional flow of a suspension of neutrally buoyant rigid particles in a Newtonian fluid between two rigid parallel planes in steady relative shearing motion. The expression to calculate the bulk stress of suspensions, presented in this section, is valid for dilute as well as non-dilute suspensions. Let the distance between the rigid parallel planes be large as compared to the particle size. Assuming the wall effects to be negligible and the flow to be homogeneous, Batchelor (1970) proposed the following expression (presented in a non-dimensional form) for the bulk stress, $\mathbf{\Sigma}$, in a suspension

$$\begin{aligned}\mathbf{\Sigma} &= -\mathbf{1}\frac{1}{A}\left(\int_{A-\mathbf{\Sigma}A_0} p\,\mathrm{d}A\right) + \overline{\mathbf{A}} + \frac{1}{A}\sum_{\text{all particles}}\int_{A_0}\boldsymbol{\sigma}\,\mathrm{d}A - \frac{\mathrm{Re}}{A}\int_A \rho\mathbf{u}'\mathbf{u}'\,\mathrm{d}A \\ &= -\mathbf{1}\frac{1}{A}\left(\int_{A-\mathbf{\Sigma}A_0} p\,\mathrm{d}A\right) + \overline{\mathbf{A}} + \mathbf{\Sigma}^{\mathrm{p}},\end{aligned} \tag{2}$$

where the ergodic assumption is made. A is the area of the unit cell over which the averaging is done, A_0 is the area of a single particle in the cell, $\boldsymbol{\sigma}$ is the stress at a point in the suspension, $\mathbf{\Sigma}^{\mathrm{p}}$ is the contribution to the bulk stress due to the presence of the particles, $\mathbf{u}' = \mathbf{u} - \overline{\mathbf{u}}$ is the velocity disturbance, $\overline{\mathbf{u}}$ is the average velocity at a point and $\overline{\mathbf{A}}$ is the average strain-rate tensor in the cell. Only the shear components of $\overline{\mathbf{A}}$ are non-zero.

The stress inside a particle is not defined by any constitutive equation. In order to evaluate the integral of stress over the particle domain in Eq. (2), we consider the particle phase to be a fluid subjected to the rigidity constraint. The momentum equation for the particle phase is

$$\rho\frac{\mathrm{d}\mathbf{u}}{\mathrm{d}t} = \nabla\cdot\boldsymbol{\sigma} \tag{3}$$

at each point in the particle domain. The stress inside the particle domain in Eq. (3) can be considered to be due to the presence of the rigidity constraint (Patankar et al., 2000). This is similar to the presence of pressure in an incompressible fluid. Using the divergence theorem and Eq. (3) we get (Batchelor, 1970)

$$\int_{A_0}\boldsymbol{\sigma}\,\mathrm{d}A = \int_{\Gamma_0}\boldsymbol{\sigma}\cdot\mathbf{n}\mathbf{x}\,\mathrm{d}\Gamma - Re\int_{A_0}\frac{\mathrm{d}\mathbf{u}}{\mathrm{d}t}\mathbf{x}\,\mathrm{d}A, \tag{4}$$

where Γ_0 is the particle boundary. This expression should be evaluated for each particle in the unit cell. By invariance of material response if we assume that the left-hand side of Eq. (4) is independent of the choice of the coordinate system, then the right-hand side is also independent; thus

we may choose for convenience a different origin for each particle if both the terms on the right-hand side are retained. We choose to select the center of the particle as the origin to calculate the terms in Eq. (4). For a homogeneous Couette flow $\mathbf{\Sigma}^{\mathrm{p}}$ is then given by (Patankar, 1997)

$$\mathbf{\Sigma}^{\mathrm{p}} = \frac{1}{A}\sum_{\text{all particles}}\int_{\Gamma_0}\boldsymbol{\sigma}\cdot\mathbf{n}\mathbf{x}\,\mathrm{d}\Gamma - \frac{\pi Re}{A}\sum_{\text{all particles}}\left\{(\mathbf{U}-\bar{\mathbf{u}}_{\mathrm{p}})(\mathbf{U}-\bar{\mathbf{u}}_{\mathrm{p}}) + \frac{1}{2}\left(\omega+\frac{1}{2}\right)\begin{bmatrix}1 & 0\\ 0 & 0\end{bmatrix}\right\} - \frac{Re}{A}\int_{A-\mathbf{\Sigma}A_0}\mathbf{u}'\mathbf{u}'\,\mathrm{d}A, \tag{5}$$

where $\bar{\mathbf{u}}_{\mathrm{p}}$ is the undisturbed velocity at the location of the particle center and ω is the angular velocity of the particle. Lin et al. (1970) used similar expressions to evaluate the particle stress for a three-dimensional case. The bulk stress in a homogeneous suspension between two parallel plates can be calculated using Eqs. (2) and (5). The area integrals include the layers adjoining the two rigid boundaries. Batchelor (1970) states that these layers *must be excluded from the range of integration in any space average if it is to be equal to the ensemble average. However, the two layers are thin, and, provided the distance between the rigid planes is large compared with the particle dimensions, they make a negligible contribution to the integrals*.

The bulk stress of a homogeneous suspension between two parallel plates can also be calculated by integrating forces on the boundaries of the domain. The expression for the average stress in the domain is given by

$$\begin{aligned}\int_A\boldsymbol{\sigma}\,\mathrm{d}A &= \int_\Gamma\boldsymbol{\sigma}\cdot\mathbf{n}\mathbf{x}\,\mathrm{d}\Gamma - Re\int_A\nabla\cdot\boldsymbol{\sigma}\mathbf{x}\,\mathrm{d}A = \int_\Gamma\boldsymbol{\sigma}\cdot\mathbf{n}\mathbf{x}\,\mathrm{d}\Gamma - Re\int_A\left(\frac{\partial\mathbf{u}}{\partial t}+\nabla\cdot(\mathbf{u}\mathbf{u})\right)\mathbf{x}\,\mathrm{d}A\\ &= \int_\Gamma\boldsymbol{\sigma}\cdot\mathbf{n}\mathbf{x}\,\mathrm{d}\Gamma - Re\int_A\left(\frac{\partial\mathbf{u}'}{\partial t}+\nabla\cdot(\bar{\mathbf{u}}\mathbf{u}')+\nabla\cdot(\mathbf{u}'\bar{\mathbf{u}})+\nabla\cdot(\mathbf{u}'\mathbf{u}')\right)\mathbf{x}\,\mathrm{d}A,\end{aligned} \tag{6}$$

where Γ includes the periodic boundary and the walls of the channel and we note that $\partial\bar{\mathbf{u}}/\partial t + \nabla\cdot(\bar{\mathbf{u}}\bar{\mathbf{u}}) = \mathbf{0}$ at steady state. By applying the divergence theorem we get

$$\int_A\boldsymbol{\sigma}\,\mathrm{d}A = \int_\Gamma\boldsymbol{\sigma}\cdot\mathbf{n}\mathbf{x}\,\mathrm{d}\Gamma - \underline{Re\int_A\left(\frac{\partial\mathbf{u}'}{\partial t}\right)\mathbf{x}\,\mathrm{d}A} + \underline{Re\int_A[(\bar{\mathbf{u}}\mathbf{u}')+(\mathbf{u}'\bar{\mathbf{u}})]\,\mathrm{d}A} + Re\int_A(\mathbf{u}'\mathbf{u})\,\mathrm{d}A - \underline{\underline{Re\int_\Gamma[\bar{\mathbf{u}}(\mathbf{u}'\cdot\mathbf{n})+\mathbf{u}'(\bar{\mathbf{u}}\cdot\mathbf{n})+\mathbf{u}'(\mathbf{u}'\cdot\mathbf{n})]\mathbf{x}\,\mathrm{d}\Gamma}},$$

or

$$\mathbf{\Sigma} = \frac{1}{A}\left(\int_A\boldsymbol{\sigma}\,\mathrm{d}A - Re\int_A(\mathbf{u}'\mathbf{u}')\,\mathrm{d}A\right) = \frac{1}{A}\int_\Gamma\boldsymbol{\sigma}\cdot\mathbf{n}\mathbf{x}\,\mathrm{d}\Gamma, \tag{7}$$

where the terms marked by double lines vanish due to the boundary conditions. The terms marked by a single line vanish with the assumptions that $\int_0^L\mathbf{u}'(x,y)\,\mathrm{d}x = \mathbf{0}$ and $\int_0^D\mathbf{u}'(x,y)\,\mathrm{d}y = \mathbf{0}$, where the x- and y-directions are as shown in Fig. (1). The expression for the bulk stress in Eq. (7) has been used to study the rheology of suspensions in the creeping flow limit (Zhou and Pozrikidis, 1993). In that case, Eq. (7) follows directly from the divergence theorem since $\nabla\cdot\boldsymbol{\sigma} = \mathbf{0}$. The alternate expression in Eq. (7) is subjected to the same assumptions with respect to

the thin layers adjacent to the walls as those for Eqs. (2) and (5). It is necessary to calculate the average normal stress on the periodic boundary in order to obtain the first normal (bulk) stress difference using Eq. (7). This is not straightforward for simulations with large number of particles where there are particles intersecting the periodic boundary. Therefore, we prefer the equivalent form in Eqs. (2) and (5) as a general expression to calculate the bulk stress of a dilute or a non-dilute suspension.

4. Bulk stress in the dilute limit

We assume that there is no interaction between the particles in the dilute limit. Consequently, it is sufficient to find the flow field around a single particle subjected to a shear flow in an infinite body of the ambient fluid. By the symmetry of this single particle problem, within the laminar range, we have $\mathbf{U} = \bar{\mathbf{u}}_p$ (Lin et al., 1970; Patankar et al., 2001). The contribution from the translational velocity disturbance to the particle stress is equal to zero. Different particles in the averaging area, A, make a linearly additive contribution to the particle stress in Eq. (5). Thus we get

$$\boldsymbol{\Sigma}^p = \frac{\phi}{\pi}\int_{\Gamma_0} \boldsymbol{\sigma}\cdot\mathbf{n}\mathbf{x}\,\mathrm{d}\Gamma - \frac{\phi Re}{2}\left(\omega+\frac{1}{2}\right)\begin{bmatrix}1 & 0\\ 0 & 0\end{bmatrix} - \frac{\phi Re}{\pi}\int_{A-A_0}\mathbf{u}'\mathbf{u}'\,\mathrm{d}A, \tag{8}$$

where area fraction $\phi = \pi N/A$ (in a non-dimensional form). It should be noted that the contribution to the particle stress from the angular velocity deviations (with respect to the value of -0.5) is retained in Eq. (8). The non-dimensional angular velocity is equal to 0.5 only in the zero Reynolds number limit. The particle stress in Eq. (8) represents the first-order correction (with respect to the area fraction) to the bulk stress of a suspension.

Einstein (1906) gave an expression for the particle stress in the dilute limit at zero Reynolds number for a three-dimensional case. Corresponding expression for a two-dimensional case is given by (Brady, 1984; Patankar, 1997)

$$\boldsymbol{\Sigma}^p = 2\bar{\mathbf{A}}, \tag{9}$$

where the contribution from the disturbance in velocity to $\boldsymbol{\Sigma}^p$ is assumed to be zero. We note that in these analytical calculations $\int_{A-A_0}\mathbf{u}'\mathbf{u}'\,\mathrm{d}A$ is singular for the zero Reynolds number dilute limit calculations.

In our numerical investigation, we will compare the numerical values of the particle stress at finite Reynolds numbers with the value at zero Reynolds number given by Eq. (9). Qualitative comparison will also be made with the low Reynolds number correction of $O(Re^{3/2})$ to the Einstein viscosity law given by Lin et al. (1970) for dilute suspensions of spheres. They found that the inertial effects give rise to a normal stress. This will also be qualitatively compared to our two-dimensional results.

5. Numerical results

Our numerical scheme is described in detail along with the convergence results by Hu (1996) and Hu et al. (2001). This scheme solves the full non-linear Navier–Stokes equations for the fluid

in conjunction with the Newton equations of motion for the particles. A periodic mesh generation scheme (Patankar and Hu, 1996) is used to take care of the periodic nature of the channel.

We perform simulations by placing a particle at the center of a periodic channel. The channel dimensions are chosen such that the bulk stress in the dilute limit does not depend on its size. The numerical results will be presented next.

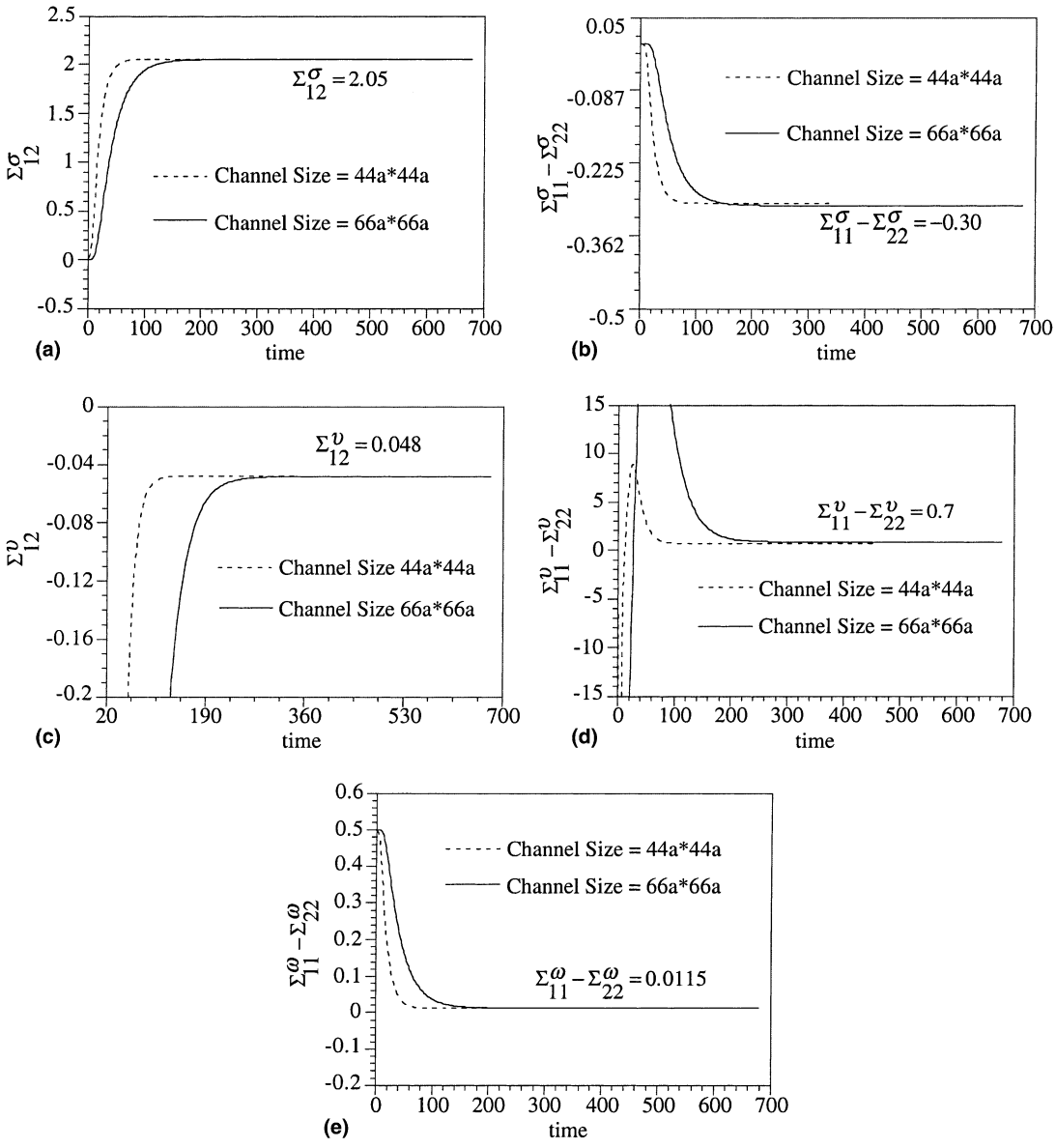

Fig. 2. Comparison of bulk properties for different channel sizes at $Re = 0.1136$. (a) Plot of Σ^{σ}_{12} as a function of time. (b) Plot of $\Sigma^{\sigma}_{11} - \Sigma^{\sigma}_{22}$ as a function of time. (c) Plot of Σ^{υ}_{12} as a function of time. (d) Plot of $\Sigma^{\upsilon}_{11} - \Sigma^{\upsilon}_{22}$ as a function of time. (e) Plot of $\Sigma^{\omega}_{11} - \Sigma^{\omega}_{22}$ as a function of time.

5.1. Bulk properties in the dilute limit

We study the effect of Reynolds number on the bulk stress in the dilute limit. We calculate the particle stress by using the following expressions:

$$\mathbf{\Sigma}^{\mathrm{p}} = \phi\mathbf{\Sigma}^{\sigma} - \frac{\phi Re}{2}\mathbf{\Sigma}^{\omega} - \phi Re\,\mathbf{\Sigma}^{v},$$

where

$$\begin{aligned}
\mathbf{\Sigma}^{\sigma} &= \frac{1}{\pi}\int_{\Gamma_0} \boldsymbol{\sigma}\cdot\mathbf{n}\mathbf{x}\,\mathrm{d}\Gamma,\\
\mathbf{\Sigma}^{\omega} &= \left(\omega+\frac{1}{2}\right)\begin{bmatrix}1 & 0\\ 0 & 0\end{bmatrix},\\
\mathbf{\Sigma}^{v} &= \frac{1}{\pi}\int_{A-A_0} \mathbf{u}'\mathbf{u}'\,\mathrm{d}A.
\end{aligned} \tag{10}$$

All the quantities in Eq. (10) are in a non-dimensional form as defined earlier.

5.2. Selection of the channel size

There is no interaction between the particles in the dilute limit. Hence it is sufficient to perform single particle simulations in which the effect of the channel size on the bulk properties is small. We ensure this by selecting the channel dimensions such that any further increase in the size does not significantly change the values of the bulk properties. This is depicted in Fig. (2) where 1 denotes the x-direction (direction of shear) and 2 denotes the y-direction (direction perpendicular to shear). All the properties have been presented as functions of the real time. In Fig. (2) we see that the steady-state values of the bulk properties do not vary significantly as the channel size is increased from $44a \times 44a$ to $66a \times 66a$. The solution for the bigger channel lags the solution for the smaller channel during the transient. This is expected because the simulations are started from rest by setting the plates in a relative motion at time $t = 0_+$. The distance δ to which the effect of wall motion propagates after it is set in motion is approximately proportional to $\sqrt{(\mu/\rho)t}$ (in a dimensional form) or $\sqrt{(1/Re)t}$ (in a non-dimensional form). The kinematic viscosity of the fluid and the Reynolds number for both the channels sizes are the same in these simulations. The distance to which the effect of wall motion must propagate to set the entire domain in a shear flow is greater in a larger channel. Consequently, it takes longer for a larger channel to reach a steady state.

Independence of the results with respect to the channel size was observed in the simulations for all non-zero values of Reynolds numbers (lowest being 0.0042). It may be verified through an approximate analysis that the 'inner' viscous region falls within the calculation domain for all the simulations at non-zero values of Reynolds numbers. This is important because in the zero Reynolds number limit the velocity disturbance due to a force in two-dimensions behaves like $\ln(r)$, where r is the radial position, and the velocity disturbance due to a force dipole decays like $1/r$, so that $\int_{A-A_0} \mathbf{u}'\mathbf{u}'\,\mathrm{d}A$ diverges.

The results presented for zero Reynolds number are calculated by considering the contribution to the particle stress from $\mathbf{\Sigma}^{\sigma}$ only. Other contributions are taken to be zero. These simulations are performed by neglecting the inertia terms in the fluid equations of motion. The non-dimensional angular velocity of the particle was found to be −0.5 for both channel sizes, which is in agreement with the analytical result. The value of $\mathbf{\Sigma}^{p}$ was also found to be in agreement with the analytical result (Eq. (9)) for both the channel sizes.

5.3. Effect of Reynolds number on $\mathbf{\Sigma}^{\sigma}$

It can be shown that the normal component of the viscous stress on the surface of a rigid body in a Newtonian fluid is zero (Bird et al., 1987). From Fig. 3(a) we observe that the primary contribution to the normal stress difference, $\Sigma^{\sigma}_{11} - \Sigma^{\sigma}_{22}$, comes from the pressure acting on the

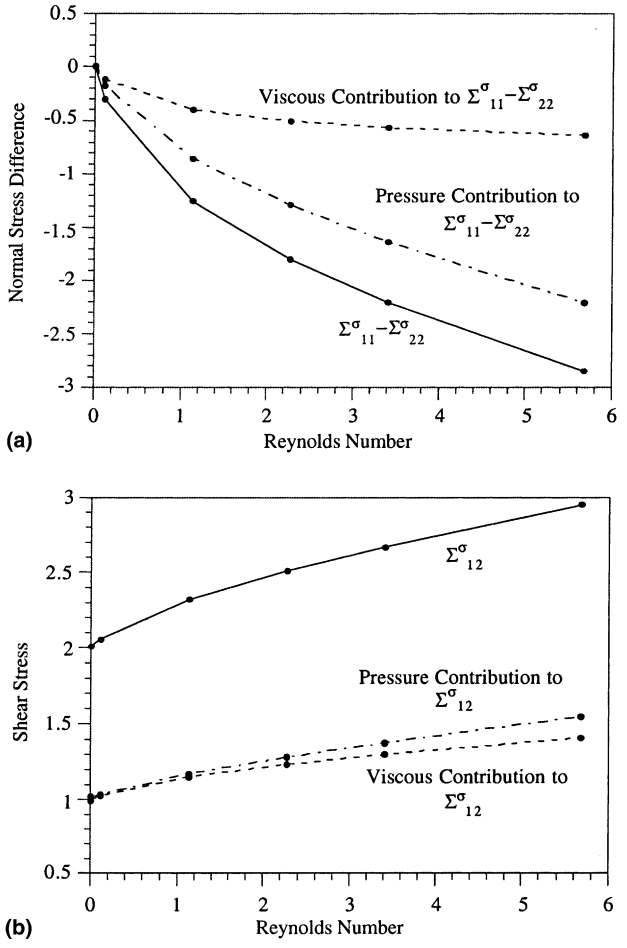

Fig. 3. Variation of particle contribution to bulk stress in the dilute limit due to the force acting on the particle surface as a function of Reynolds number. (a) Normal stress difference as a function of Reynolds number. (b) Shear stress as a function of Reynolds number.

surface of the particle. This normal stress difference is negative and increases in magnitude as the Reynolds number increases (Fig. 3(a)). The shear stress, Σ_{12}^{σ}, is seen to increase with the Reynolds number thus showing shear thickening behavior.

In the limit of zero Reynolds number the only contribution to the particle stress, $\mathbf{\Sigma}^{\mathrm{p}}$, comes from $\mathbf{\Sigma}^{\sigma}$. Fig. 3 shows that our numerical results are in agreement with the analytical result (Eq. (9)).

$\Sigma_{11} - \Sigma_{22}$ is the first normal stress difference and $\Sigma_{22} - \Sigma_{33}$ the second normal stress difference, where $\mathbf{\Sigma}$ is the overall stress and 3 is the z-direction in case of a general three-dimensional problem. In a two-dimensional case the second normal stress difference is not defined. For most polymers the first normal stress difference is positive whereas the second normal stress difference is negative and an order of magnitude smaller than the first normal stress difference (Bird et al., 1987). In order to maintain a steady shear flow between two parallel plates, a normal force must be applied to the plates to prevent them from separating when the fluid is polymeric. It should be noted that the second normal stress difference for suspensions in a three-dimensional case may not be small (Sangani et al., 1996).

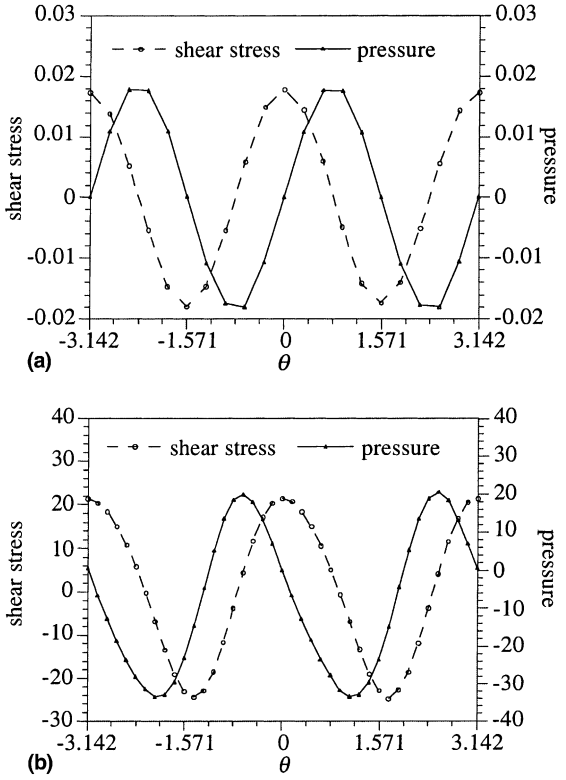

Fig. 4. Variation of dimensional shear stress and pressure with angular position, θ, on the surface of the particle. Pressure is taken to be zero at $\theta = 0$. Shear stress is directed in the anti-clockwise sense. (a) $Re = 0$, (b) $Re = 2.273$, (c) A long rectangular particle at the center of a channel in a steady Couette flow between two parallel plates. The dotted line represents the undisturbed velocity profile whereas the solid line represents the velocity profile in the presence of the long particle. The shear-rate inside the rectangular particle is zero.

Suspensions of rigid particles in a Newtonian fluid at finite Reynolds numbers exhibit a normal stress difference due to the particle contribution to the bulk stress. We observe (Fig. 3(a)) that the contribution to the first normal stress difference due to the stresslet term ($\mathbf{\Sigma}^{\sigma}$) is negative. This implies that, to maintain a steady shear flow, the plates should be pulled away from the suspension to prevent them from moving towards one another. This behavior is qualitatively different from that shown by polymers. The physical basis for this behavior may be understood through the following simplistic argument.

Consider a particle in a Newtonian fluid subjected to a shear flow between two parallel plates (Fig. 1). Let the channel be large enough for the dilute limit results to be valid. The dilute limit results are typically seen to be applicable for $\phi < 2\%$ (Batchelor, 1967). Fig. 4(a) shows the distribution of the shear stress and the pressure on the surface of the particle at zero Reynolds number. We observe that the distribution of the shear stress has extrema at $\theta = 0,\ \pi\ (-\pi),\ \pi/2$ and $-\pi/2$. At zero Reynolds number the magnitudes of these extrema are the same. The pressure is zero at each of these locations. The average pressure on the plates and on a plane (far from the particle) perpendicular to the axis of the channel is the same. As a result the first normal stress difference is zero. At higher Reynolds numbers, the magnitudes of the extrema of the shear stress at $\theta = \pi/2$ and $-\pi/2$ are greater than those at $\theta = 0$ and π (Fig. 4(b)). The streamlines are more crowded at $\theta = \pi/2$ and $-\pi/2$. The inertial effects cause the pressure to be lower at $\theta = \pi/2$ and $-\pi/2$ than at $\theta = 0$ and π (Fig. 4(b)). This causes lower pressure in the fluid between the particle and the plates. The average pressure on the plates is less than that on a plane perpendicular to the channel axis. This results in a net 'suction force' on the plates, i.e. a negative first normal stress difference. This effect becomes stronger as the Reynolds number is increased.

Next, we consider the long particle model of Joseph et al. (2001), also presented by Patankar et al. (2001), to understand the shear thickening of a dilute suspension. The circular particle of radius a is replaced by a long rectangle whose short side is $2a$ (Fig. 4(c)).

Assuming the shear-rate inside the particle to be zero, the magnitude of the shear-rate between the particle and the plates is given by

$$\frac{\mathrm{d}u}{\mathrm{d}y} = \frac{V/2}{D/2 - a}. \tag{11}$$

The long particle cannot rotate but the effect of rotation can be expressed by allowing a shear-rate, in the long body as if it were a viscous fluid, equal to the angular velocity of the circular particle. A long particle without shear corresponds to a circular particle for which the rotation is suppressed. For a long particle with a prescribed shear-rate

$$\frac{\mathrm{d}u}{\mathrm{d}y} = \frac{V/2 + \omega a}{(D/2 - a)} = \dot{\gamma}\left[1 + \frac{\{0.5 + (0.5 + \omega/\dot{\gamma})\}\varphi}{1 - \phi}\right], \tag{12}$$

i.e. in the dilute limit

$$\eta = \eta[1 + \{0.5 + (0.5 + \omega/\dot{\gamma})\}\phi] = \eta[1 + \{0.5 + \omega_s\}\phi],$$

where $\dot{\gamma} = V/D$ is the average shear-rate between the plates, $\phi = 2a/D$ is the area fraction of the long particle and η_s is the effective viscosity. The channel size is large in the dilute limit. It should be noted that ω is negative for rotations (due to the applied shear) in the clockwise direction. At

zero Reynolds number $\omega_s = 0$. Eq. (12) predicts that shear thickening will be observed if ω_s is positive and increases as the Reynolds number is increased.

Fig. 5(a) shows the variation of the non-dimensional angular velocity of the circular particle vs. the Reynolds number. At zero Reynolds number the angular velocity is −0.5; in agreement with the analytical result. The magnitude of the angular velocity decreases as the Reynolds number is increased, i.e. ω_s is positive and increases with the Reynolds number (Fig. 5(a)). The qualitative prediction of Eq. (12) is therefore in agreement with the observed shear thickening of the dilute suspension. A smaller angular velocity at higher Reynolds numbers gives rise to a steeper gradient of velocity between the particle and the plates. This causes shear thickening of the suspension. Lin et al. (1970) also obtained similar behavior due to the effect of inertia at low Reynolds numbers (<1).

Ding and Aidun (2000) reported the angular velocities of a cylinder in shear flow at different Reynolds numbers. They compared their numerical results with the experimental results of Poe and Acrivos (1975). Fig. 5(b) shows comparison between our results and those of Poe and Acrivos (1975) on a log–log plot. The agreement is good.

It is interesting to note that Poe and Acrivos (1975) could not perform steady flow experiments for Reynolds numbers (based on particle radius) higher than 5.75 due to appearance of flow

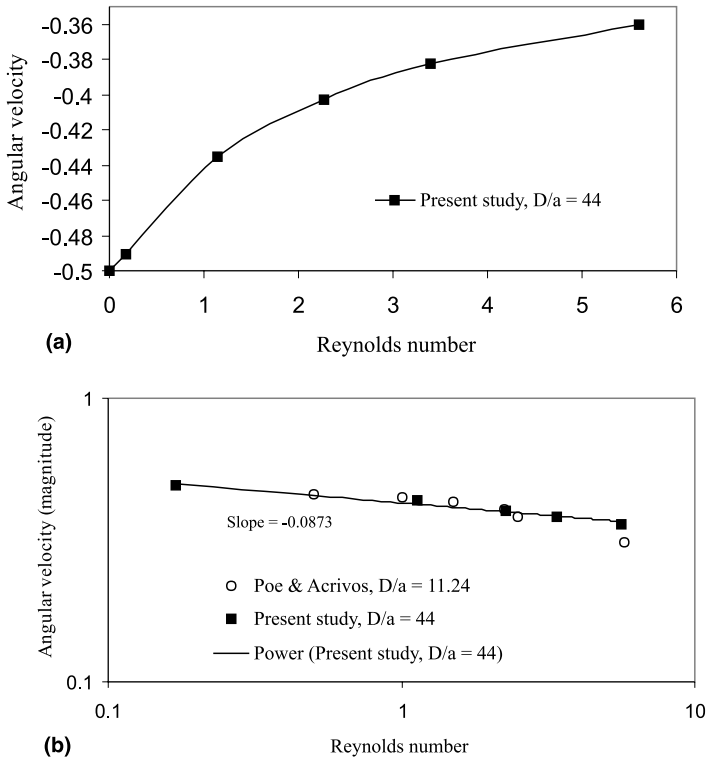

Fig. 5. (a) Non-dimensionalized angular velocity, ω, as a function of Reynolds number. (b) Magnitude of the non-dimensional angular velocity as a function of Reynolds number. Comparison between present study and the experimental results of Poe and Acrivos (1975) are presented.

instabilities. In our simulations we encountered convergence problems for *Re* greater than 5.6 which may also be due to instabilities. This needs further investigation. An alternate cause of our convergence problem may be linked to the channel size. Our channel size is 44 times the particle radius, hence the channel Reynolds number is high giving rise to instabilities.

5.3.1. *Effect of Reynolds number on* $\mathbf{\Sigma}^{\omega}$ *and* $\mathbf{\Sigma}^{\upsilon}$

Fig. 6 shows the effect of Reynolds number on the contribution to the bulk stress due to velocity disturbance. We observe that $-Re\Sigma_{12}^{\upsilon}$ shows a shear thickening behavior at lower Reynolds

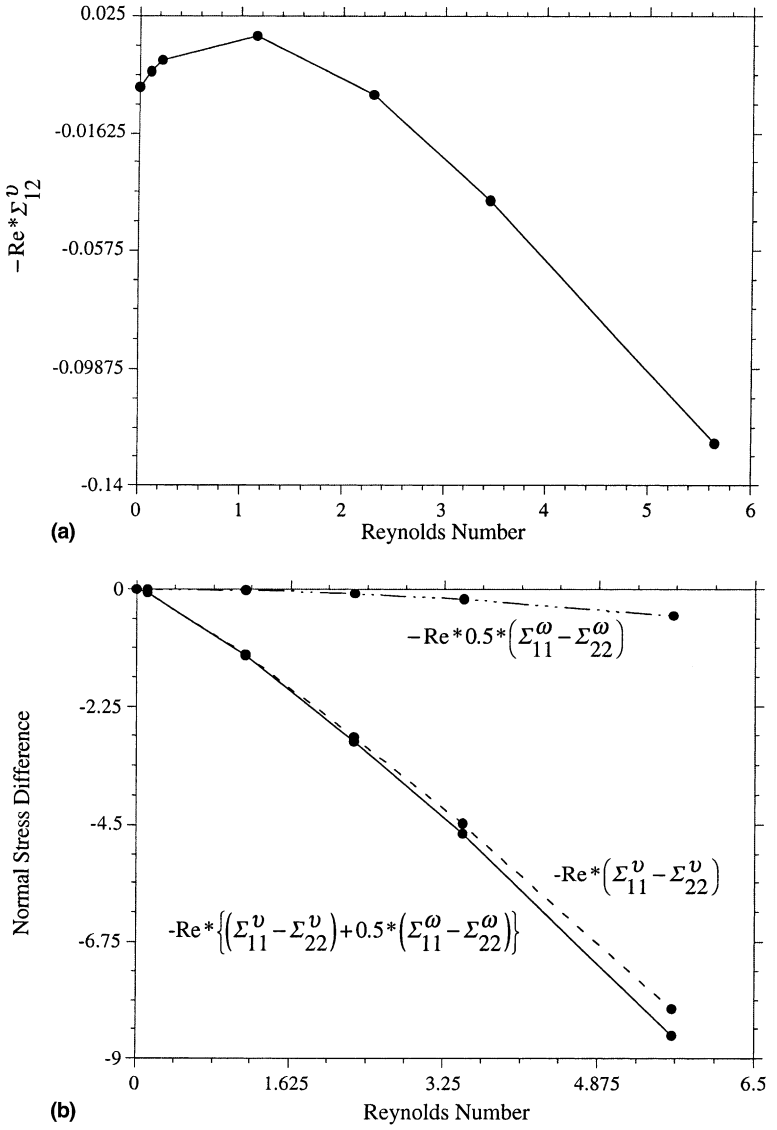

Fig. 6. Disturbance contributions to the particle stress. (a) Shear stress component as a function of Reynolds number. (b) Normal stress differences as a function of Reynolds number.

numbers and a shear thinning behavior at higher Reynolds numbers. This contribution to the bulk stress is small in comparison to the stresslet contribution presented earlier. As a result the overall behavior of the shear stress is shear thickening and will be presented shortly.

Fig. 6(b) shows that the contribution to the first normal stress difference due to the angular velocity deviation is negligible as compared to the contribution from the velocity disturbance in the fluid. This normal stress difference is negative and increases in magnitude as the Reynolds number increases.

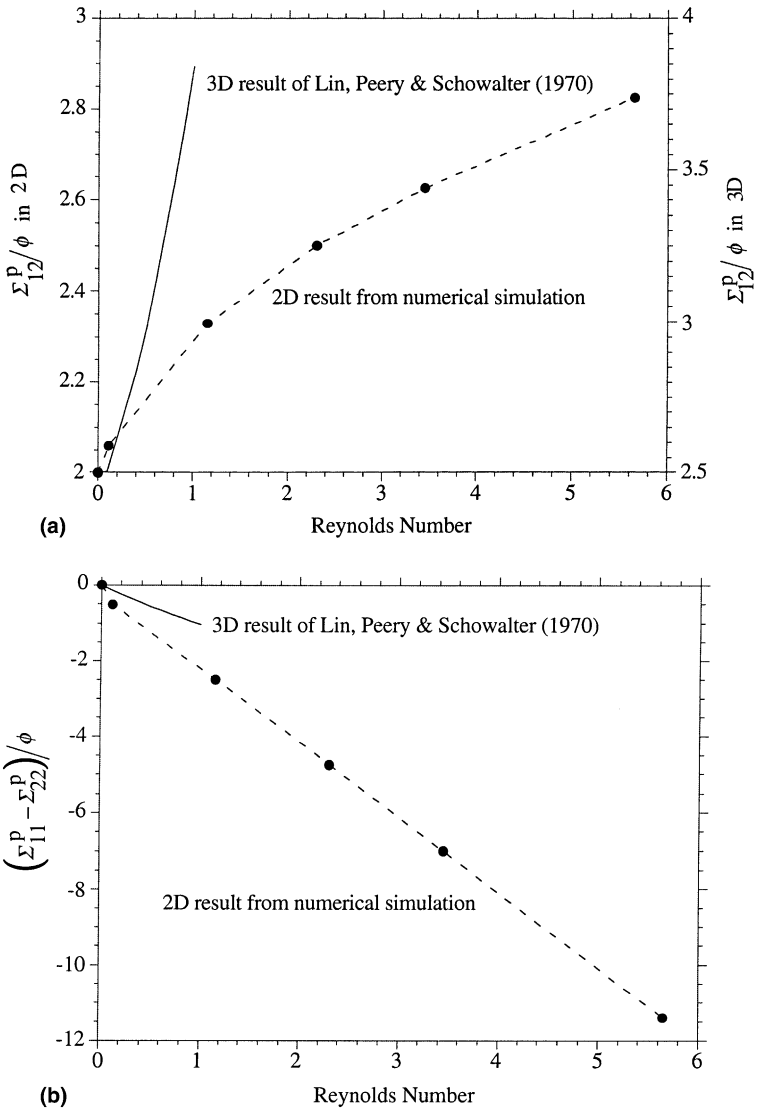

Fig. 7. Variation of particle stress as a function of Reynolds number. (a) Variation of shear stress. (b) Variation of the first normal stress difference.

5.3.2. Overall trend of the particle stress

Fig. 7 shows the variation of the particle stress as a function of the Reynolds number. We notice a shear thickening behavior of the shear stress and a negative first normal stress difference. Lin et al. (1970) studied the effect of inertia on the rheology of suspensions of rigid spheres in a Newtonian fluid. They used perturbation techniques to obtain the flow field in the vicinity of a single particle in a Newtonian fluid subjected to a shear flow. Their results are applicable in the dilute limit at low Reynolds numbers (<1) and are shown in Fig. 7 up to $Re = 1$. They observed a shear thickening behavior and a negative first normal stress difference as well. Our results for a two-dimensional case are valid at finite Reynolds numbers without being restricted to values less than one. An extension of our approach to a three-dimensional case is in progress and can provide valuable information about three-dimensional suspension rheology at higher values of Reynolds numbers.

Similar trends were observed for non-dilute suspensions from preliminary simulations at higher concentrations reported by Patankar (1997).

6. Conclusions

In this paper we have studied the effect of Reynolds number on the macroscopic properties of a suspension of rigid cylinders in a Newtonian fluid using numerical simulations. This investigation was carried out in the dilute limit.

It was seen that the effective viscosity of the suspension shear thickens, i.e. the effective viscosity increases as the Reynolds number is increased. This is because the non-dimensionalized angular velocity of the particle decreases as the Reynolds number is increased. This causes steeper gradients of velocity between the walls of the channel and the particle thus giving rise to higher shear stress at the channel walls. Dilute limit investigation also showed that finite Reynolds number causes negative first normal stress difference. This implies that to maintain a steady shear flow of a suspension of rigid particles in a Newtonian fluid between two parallel plates, the plates should be pulled away from the suspension to prevent them from moving towards one another. This was explained by the presence of lower pressure between the channel walls and the particles due to inertial effects. Low pressure induces suction on the plates on the channel, thus pulling them towards one another.

Suitable experimental data are not available to directly compare the predictions of our simulations and should become a part of further investigation. Our investigation is based on two-dimensional simulations. There can be some qualitative differences between these predictions and the three-dimensional case. The methodology introduced here can easily be extended to three dimensions and is the focus of our future investigation.

Acknowledgements

This work was supported by the National Science Foundation under an HPCC Grand Challenge Grant ECS-9527123 and CTS 94-10022 and by the Research Foundation of the University

of Pennsylvania. NAP would like to acknowledge the support from Northwestern University through the startup funds.

References

Batchelor, G.K., 1967. An Introduction to Fluid Dynamics. Cambridge University Press, Cambridge, UK.
Batchelor, G.K., 1970. The stress system in a suspension of force-free particles. J. Fluid Mech. 41, 545.
Batchelor, G.K., 1974. Transport properties of two-phase materials with random structure. Ann. Rev. Fluid Mech. 6, 227.
Batchelor, G.K., 1976. Developments in microhydrodynamics. In: Koiter, W. (Ed.), Theoretical and Applied Mechanics. North-Holland, Amsterdam, p. 33.
Bird, R.B., Armstrong, R.C., Hassager, O., 1987. In: Dynamics of Polymeric Liquids, vol. 1. Wiley/Interscience, New York.
Brady, J.F., 1984. The Einstein viscosity correction in *n* dimensions. Int. J. Multiphase Flow 10, 113.
Brady, J.F., 1993. Stokesian dynamics simulations of particulate flows. In: Roco, M.C. (Ed.), Particulate Two-Phase Flow. Butterworth/Heinemann, New York, p. 912.
Brady, J.F., Bossis, G., 1988. Stokesian dynamics. Ann. Rev. Fluid Mech. 20, 111.
Brenner, H., 1974. Rheology of a dilute suspension of axisymmetric Brownian particles. Int. J. Multiphase Flow 1, 195.
Davis, R.H., Acrivos, A., 1985. Sedimentation of noncolloidal particles at low Reynolds numbers. Ann. Rev. Fluid Mech. 17, 91.
Ding, E.J., Aidun, C.K., 2000. The dynamics of scaling law for particles suspended in shear flow with inertia. J. Fluid Mech. 423, 317.
Einstein, A., 1906. Eine neue Bestimmung der Moleküldimensionen. Ann. Phys. 19, 289 (34, 591, 1911).
Foss, D.R., Brady, J.F., 2000. Structure, diffusion and rheology of Brownian suspensions by Stokesian dynamic simulations. J. Fluid Mech. 407, 167.
Hu, H.H., 1996. Direct simulation of flows of solid–liquid mixtures. Int. J. Multiphase Flow 22, 335.
Hu, H.H., Patankar, N.A., Zhu, M.-Y., 2001. Direct numerical simulations of fluid–solid systems using the Arbitrary–Lagrangian–Eulerian technique. J. Comput. Phys. 169, 427.
Jeffrey, D.J., Acrivos, A., 1976. The rheological properties of suspensions of rigid particles. AIChE J. 22, 417.
Joseph, D.D., Ocando, D., Huang, P.Y., 2001. Slip velocity and lift. J. Fluid Mech. (to appear).
Kang, S.Y., Sangani, A.S., Tsao, H.K., Koch, D.L., 1997. Rheology of dense bubble suspensions. Phys. Fluids 9, 1540.
Koch, D.L., 1990. Kinetic-theory for a monodisperse gas–solid suspension. Phys. Fluids A 2, 1077.
Lin, C., Peery, J.H., Schowalter, W.R., 1970. Simple shear flow round a rigid sphere: inertial effects and suspension rheology. J. Fluid Mech. 44, 1.
Marchioro, M., Tanksley, A., Prosperetti, A., 2000. Flow of spatially non-uniform suspensions. Part I: Phenomenology. Int. J. Multiphase Flow 26, 783.
Marchioro, M., Tanksley, A., Wang, W., Prosperetti, A., 2001. Flow of spatially non-uniform suspensions. Part II: Systematic derivation of closure relations. Int. J. Multiphase Flow 27, 237.
Patankar, N.A., 1997. Numerical simulation of particulate two-phase flow. Ph.D. Thesis, University of Pennsylvania.
Patankar, N.A., Hu, H.H., 1996. Two-dimensional periodic mesh generation. In: Proceedings of the 5th International Conference on Numerical Grid Generation in Computational Field Simulations, Starkville, USA, p. 1175.
Patankar, N.A., Huang, P.Y., Ko, T., Joseph, D.D., 2001. Lift-off of a single particle in Newtonian and viscoelastic fluids by direct numerical simulation. J. Fluid Mech. 438, 67.
Patankar, N.A., Singh, P., Joseph, D.D., Glowinski, R., Pan, T.-W., 2000. A new formulation of the distributed Lagrange multiplier/fictitious domain method for particulate flows. Int. J. Multiphase Flow 26, 1509.
Poe, G.G., Acrivos, A., 1975. Closed-streamline flows past rotating single cylinders and spheres: inertia effect. J. Fluid Mech. 72, 605.
Russel, W.B., 1980. Review of the role of colloidal forces in the rheology of suspensions. J. Rheol. 24, 287.
Ryskin, G., Rallison, J.M., 1980. The extensional viscosity of a dilute suspension of spherical particles at intermediate microscale Reynolds numbers. J. Fluid Mech. 99, 513.

Sangani, A.S., Mo, G.B., Tsao, H.K., Koch, D.L., 1996. Simple shear flows of dense gas-solid suspensions at finite Stokes numbers. J. Fluid Mech. 313, 309.

Sangani, A.S., Prosperetti, A., 1993. Numerical simulation of the motion of particles at large Reynolds numbers. In: Roco, M.C. (Ed.), Particulate Two-Phase Flow. Butterworth/Heinemann, New York, p. 971.

Zhou, H., Pozrikidis, C., 1993. The flow of suspensions in channels: single files of drops. Phys. Fluids A 5, 311.